

INFLUENCE OF THE MICRO-TOPOGRAPHY ON RADARSAT-1 AND PALSAR BACKSCATTERING RESPONSES FOR DISCRIMINATION OF SURFICIAL GEOLOGIC UNITS IN THE CURAÇÁ VALLEY (BAHIA).

Waldir Renato Paradella¹
Arnaldo de Queiroz da Silva¹
Sheila Soraya Alves Knust²
Tiago Nunes Rabelo¹
Athos Ribeiro dos Santos¹
Camilo Daleles Rennó¹
Cleber Gonzalez de Oliveira¹
Thiago Gonçalves Rodrigues¹

¹Instituto Nacional de Pesquisas Espaciais – INPE
12227-010 - São José dos Campos - SP, Brasil
{waldir, athos, cleber, tiago, thiagogr@ltd.inpe.br;
arnaldo@dsr.inpe.br; camilo@dpi.inpe.br}

²Serviço Geológico do Brasil-CPRM (Sureg-GO)
74170-110 – Goiânia – GO, Brasil
sknust@go.cprm.gov.br

Abstract. SAR images have been successfully used for geological applications in the moist environments of Brazil. However, for semi-arid environment researches dealing with radar are still rare. The Cu-rich district of Curaçá Valley (Ba) is characterized by a flat topography with residual soils and low to moderate Caatinga vegetation cover. Geologically, the Valley is part of the Salvador-Curaçá belt, a Paleoproterozoic N-S trending, granulite-amphibolite belt in the São Francisco Craton. The lithological units are grouped as Archean gneisses and granulites interbedded with ferruginous rocks, quartzites, amphibolites, mafic-ultramafic intrusives and Upper Proterozoic marbles/limestones, schists, and phyllites. The objective of the investigation was to evaluate the influence of micro-topography on RADARSAT-1 and PALSAR responses as an aid to discriminating surficial geologic units. The images were acquired under distinct look-azimuth (ascending, descending passes) and variable incidence. Four RADARSAT-1 (F2 ascending, S2 and S7 ascending, S7 descending) and one PALSAR (FBD, descending) images were used. The relationship between sigma nought (σ^0) and rms-heights (h_{rms}) and correlation-length (L_c), revealed that the use of micro-topography for characterization of geological surfaces is limited, given by a weak to moderate linear correlation ($R_2^2 \leq 0.50$) for both SAR data. For RADARSAT-1, the dependence of σ^0 on h_{rms} and L_c increased from steeper to shallower incidence independently of the look-azimuth. For PALSAR, the maximum value of R_2^2 (0.51) for h_{rms} and L_c was obtained for cross-pol (L-HV). Volume scattering related to the vegetation with green foliage probably contributed to this performance.

Key-words: RADARSAT-1, ALOS-PALSAR, surface roughness, rock discrimination, Curaçá Valley, Bahia.

1. Introduction

A reasonable amount of airborne and orbital Synthetic Aperture Radar (SAR) data, with distinct characteristics (frequency, polarization, viewing terrain geometry, spatial resolution, etc.) has been evaluated for geological applications over the moist environments of the Amazon Region. However, in Brazilian semi-arid regions researches dealing with the use of SAR are still absent. In an environment characterized by low to sparse vegetation cover and dry conditions, SAR systems are sensitive to the electrical and morphological properties of the terrain surface. These conditions favor a SAR investigation since is often difficult to make a direct relationship between rock alteration products with radar responses.

The dielectric constant of surfaces related to rock types and alteration products is dependent on chemical composition, porosity and water content of surface/subsurface layers

(Ulaby et al. 1990). In semi-arid regions, precipitation is generally concentrated over a short period of time and irregularly distributed over small areas. Depending on the particular circumstances, moisture may produce higher SAR responses from wet terrains favoring the discrimination of the rock alteration products (Rabelo et al. 2007). But in general, the influence of moisture is comparatively small and the microwave responses tend to be controlled by morphological properties of the terrain surface (Deroin et al. 1997).

The sensitivity of the SAR backscatter to geological surface roughness still remains to be determined quantitatively in natural conditions. Three scales of terrain roughness can be considered when dealing with SAR data: macro-topography, micro-topography, and the intermediate-scale region between these two regimes. The macro-topography is related to decameter changes in slope (tilts, broad undulations of the terrain) and orientation of surface facets being generally related to geological structures, erosional features and geomorphology (macro-texture patterns many times larger than the sensor resolution cell). The micro-topography regime comprises height variations and undulations lengths comparable to the radar wavelength and determines intensity and type (single or multiple scattering) of the scattered radar signal. The effects of the intermediate-scale region are not well known but affect both the small-scale scattering characteristics and the reradiation patterns from large-scale topography (Dierking 1999). In this paper, the dependence of the radar backscatter on micro-topography (micro-surface roughness) was quantitatively assessed based on RADARSAT-1 and PALSAR data acquired at the lower sector of the Curaçá Valley (Ba).

2. The study area

The test-site selected for the investigation, the Curaçá River Valley, is part of a Cu-rich district located in the northern part of the State of Bahia. The climate in the region is semi-arid, with average temperature around 30 °C and between 300 and 700 mm of annual rainfall occurs mainly in summer (January to March) marked by heavy showers of short duration. At such times, normally dry valleys become fast-flowing streams and flooding occurs on the low flat lands. Topographically, the area is characterized by a land surface eroded to a nearly flat plain, with altitudes ranging from 330 to 830 m above sea level. In this pediplain, the altimetric variation among watersheds is approximately 20 m. The resistance of crystalline rocks coupled with the tropical semi-arid weather leads to high run-off rates and the rapid removal of weathered material by sheet flooding. This has resulted in the dominance of the erosional process over soil formation, and, as a consequence, soils are generally shallow (30 cm to 1.5 m) but relatively fertile, except for the organic matter content. Conversely, drainage channels work as accumulation sites and tend to have deep deposits that receive a large volume of transported and partly weathered material, mainly rock fragments. The soils in the plain range from sandy to clay-rich (montmorillonites) soils that present close relationships with the substratum as demonstrated by Paradella (1983) using $\text{Ca}^{++}/\text{Mg}^{++}$ determinations in several soil horizons. Pavements are commonly covered by boulders, shattered quartz pebbles, and angular rock fragments. The dominant soils studied based on U.S. classification are Palexeralfs, Abruptic Durixeralfs, Typic Eutorrox, Lithic Torriorthents and Lithic Camborthids. Outcrops are usually found in eroded drainage channels and steep slopes.

Annual fluctuations in climatic conditions, especially rainfall, have resulted in variations in the Caatinga vegetation physiognomy and phenology, but dominant are deciduous woody shrubs (4 to 7 m in height), with moderate to low cover density, canopy structure and stratification (up to three strata). During the dry season, the xerophytism leads to the shedding of foliages, and where the canopy is dense, an apparently homogeneous grey woody mass is visually remarkable. The deciduous perennials shed their leaves in May or earlier and are dormant up to the beginning of the rainy season, around December.

Geologically, the test-site is part of the Itabuna-Salvador-Curaçá Belt (ISB), one of the four Archean crustal segments in the São Francisco Cráton. The ISB encompasses at least four groups of tonalite/trondhjemites, three with Archean (2.6 Ga) and one with Paleoproterozoic (2.1 Ga) ages (Barbosa and Sabaté, 2003). These groups are interpreted as result of tholeiitic crust fusion, but also includes charnockitic bodies (2.6 Ga) and stripes of intercalated metasediments and ocean-floor/back-arc gabbros and basalts. During the Paleoproterozoic Orogeny, ISB and the other three Archean blocks (Gavião, Jequié and Serrinha) collided and resulted in the formation of an important N-S trending mountain belt, the Itabuna-Salvador-Curaçá Orogen. Geochronological data indicated that the regional metamorphism, under granulite, amphibolite and greenschist facies, is related to a crustal thickening associated with the collision process, which took place c.a. 2.0 Ga.

The northern segment of the Itabuna-Salvador-Curaçá Belt where the test-site is located is formed by a basement of tonalitic to quartz-monzodioritic composition with gabbroic levels. The basement is overlain by a sedimentary supracrustal sequence pelitic at the base and chemical at the top. The main sequences are orthogneisses and granulite facies rocks of the Caraíba Complex and metamorphosed supracrustal rocks of the Tanque Novo-Ipirá Complex of NeoArchaen age or older (Kossin et al. 2003). Covering these rocks, plataformal sequences (glacial and pelitic-carbonatic) of the São Francisco Supergroup took place during the Late Neoproterozoic. The Caraiba copper orebody as well as other small copper deposits in the Valley are hosted in mafic-ultramafic rocks within the supra-crustal sequence with reserves exceeding 150 million tones of ore (0.5 to 1.0% average Cu grade). Massive and disseminated sulfides are associated with pyroxenites and weak disseminated sulfides to norites, gabbro-norites and anorthosites. The Curaçá Valley was mapped in the scale of 1:50.000 (Delgado and Souza 1975) and the lithological units can be grouped as Archean gneissic and granulitic assemblages, interbedded with ferruginous rocks, quartzites, amphibolites, mafic-ultramafic intrusives, and a sequence of Upper Proterozoic metasediments (marbles/limestones, schists, and phyllites). These units show structural grain (foliation) with an N-S trend and metamorphism ranging from greenschists to granulite facies. The main mapped rock units in the study area are shown in Figure 1.

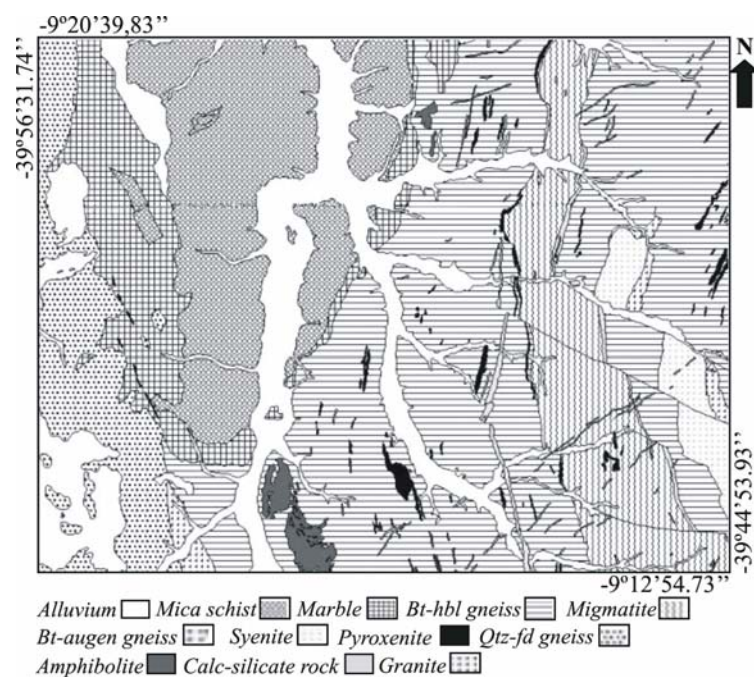


Figure 1. Lithological units of the study area (source: Delgado and Souza 1974)

3. SAR dataset

The investigation was based on four RADARSAT-1 and one PALSAR images collected under distinct look-azimuth (ascending and descending passes) and variable incidence (Figure 2). The SAR data were acquired on September and October 2003 (RADARSAT-1) and May 2007 (PALSAR), and were available as single or multi-looks, amplitude image, 16-bit format (the specific types of products are seen on Tables 1 and 2).

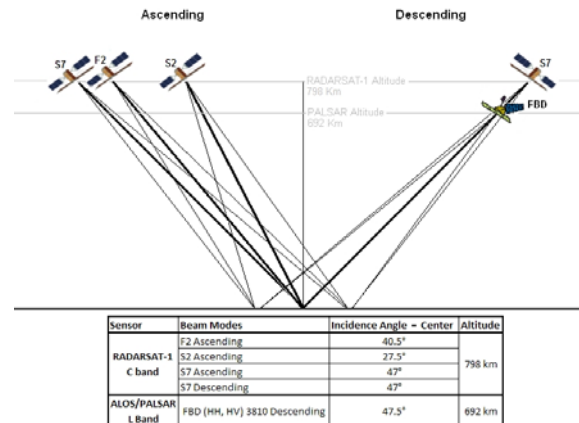


Figure 2. Scheme of the acquisition of RADARSAT-1 and PALSAR data in the study area.

Table 1. RADARSAT-1 data characteristics.

images	Standard (Beam 2)	Fine (Beam 2)	Standard (Beam 7)	Standard (Beam 7)
product level	SGF	SGF	SGF	SGF
polarization	C-HH	C-HH	C-HH	C-HH
look-azimuth	78° (ascending)	78° (ascending)	78° (ascending)	282° (descending)
date	17/09/2003	27/09/2003	14/10/2003	22/10/2003
incidence	27.5°	38.5°	47°	47°
looks	1 x 4	1 x 1	1 x 4	1 x 4
resolution (m)	22 x 27	8.7 x 8.4	20.09 x 27	20.09 x 27
format	CEOS	CEOS	CEOS	CEOS

Table 1. ALOS-PALSAR data specification.

images	FBD (Fine Beam Dual)
product level	1.5
polarization	L-HH, L-HV
look-azimuth	282° (descending)
date	02/05/2007
incidence	47.45°
looks	1 x 4
spatial resolution (m)	4.49 x 9.6
format	1.5 UD CEOS JAXA

An average rainfall value of almost nil (0.2 mm) for the interval of Aug-Oct of 2003, previously to the RADARSAT-1 passes, was recorded by the Bebedouro Agrometeorological Station of the Brazilian Agricultural Research Corporation (EMBRAPA), 50 km from the study area. On the other hand, the precipitation values indicated a wetter condition, previously to the PALSAR acquisition, with a total of 162 mm for the period of March-May of 2007.

4. Methodological Approach

4.1 SAR processing

For RADARSAT-1, before the conversion of digital number (DN) to σ^0 , speckle suppression was applied using Enhanced-Frost filtering algorithm (7 x 7 pixels window) and incidence values for each pixel position was extracted based on the SARINCD algorithm (PCI Geomatics 10.1), which creates an array segment of incidence angle to use with a SAR gain scaling table. The DN-to- σ^0 conversion was carried out based on the SARSIGM algorithm (PCI Geomatics 10.1), which generates a calibrated radar backscatter image from the original input scaled SAR image and an array of correspondent incident angles for each pixel. In the case of PALSAR data, the σ^0 values were extracted using the equation from Shimada et al. (2007): $\sigma^0 = 10.\log_{10}(\text{DN}^2) + \text{CF}$, where CF (conversion factor) to data in amplitude is -83. The SAR images were further orthorectified using planialtimetric information from a 1:100 000 scale topographic map and a parametric model inside OrthoEngine package, which takes into account principles related to orbitography, photogrammetry, geodesy and cartography (PCI Geomatics 10.1). Finally, the images were resampled to a common pixel size through a mean filter (5 x 5 pixels window). The pixel size was defined based on the statistics of the circular error at 90% confidence (CE 90) from the orthorectification, which assure that points are represented on the images within the accuracy 90% of the time.

4.2 Field roughness measurements

Two campaigns were made in Sept 2006 and Oct 2008. It is generally assumed that micro-topography is isotropic, and the characterization of surface roughness is obtained from statistical values derived from height variations seen along transects (Verhoest et al. 2008). A meshboard technique was used, which involves inserting a thin plastic gridded board (1.2 m long x 0.2 cm height and 2-cm intervals grid) in the soil and making a picture after which it is digitized (Figure 2). Micro-topography was measured for 18 sites chosen by the geologic map and over a circle with a 60 m radius (CE 90) at each sampling location. For the field location a handheld GPS was used, and six profile measurements were made continuously at each site producing a 7.2 m long transect (multi-site database of 1.2 m profiles).

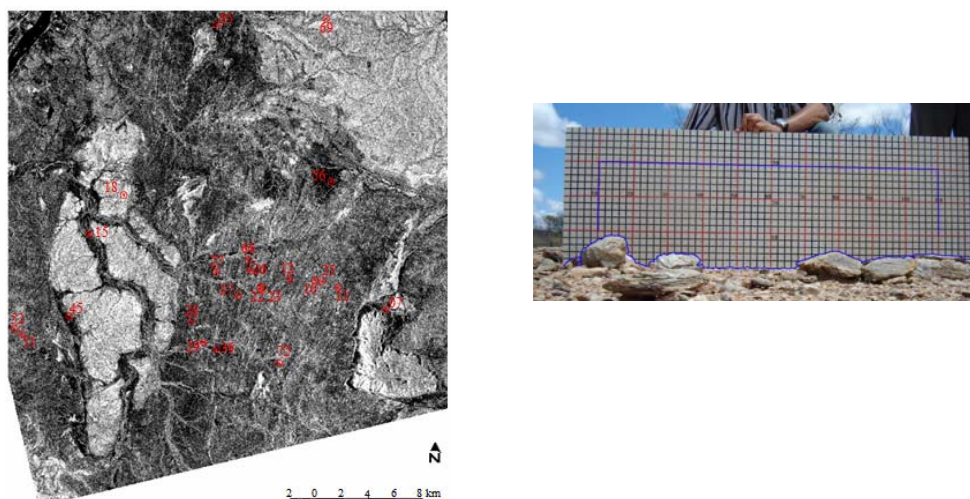


Figure 3. Location of the measurements' sites and an example of surface roughness profile.

4.3 Statistical parameters derivation (h_{RMS} and L_c)

The two parameters commonly derived from the transects and used in the study to characterize surface roughness were the standard deviation of the surface height variation (or h_{RMS}) and the surface correlation length (L_c). In other words, the vertical roughness is expressed by h_{RMS} and the horizontal roughness is described by L_c (Dierking 1999). The values of h_{RMS} and L_c were obtained from the profiles using the following equations (Ulaby et al. 1996):

$$h_{RMS} = \left[\frac{1}{N-1} \left(\sum_{i=1}^N (z_i)^2 - N(\bar{z})^2 \right) \right]^{1/2} \quad \text{where} \quad \bar{z} = \frac{1}{N} \sum_{i=1}^N z_i \quad (1)$$

L_c was calculated from the autocorrelation function for $x' = (j-1) \Delta x$, where j is an integer ≥ 1 .

$$\rho(x') = \frac{\sum_{i=1}^{N+1-j} z_i z_{j+i-1}}{\sum_{i=1}^N z_i^2} \quad \rho(l) = \frac{1}{e} \quad \text{where } e \text{ is the natural log} \quad (2)$$

In other words, the correlation length describes the horizontal distance over which the surface profile is autocorrelated with a value larger than $1/e$ (≈ 0.368).

5. Results and Discussions

The error residuals for RADARSAT-1 and PALSAR using Independent Check Points (ICPs) are given in Table 3. Taking into account the CE90 statistics of the orthorectification, the SAR images were resampled to 60 m spatial resolution. The results of σ° , h_{RMS} and L_c for the rock alteration products are given in Table 4.

Table 3. Error results for the orthorectification of RADARSAT-1 and PALSAR.

SAR	X RMS (m)	Y RMS (m)	RMS residual (m)	CE90
Fine 2 Asc.	6.48	6.67	9.29	19.51
Standard 2 Asc	16.54	17.57	24.13	50.67
Standard 7 asc	17.96	14.22	22.91	48.11
Standard 7 desc	15.52	18.13	23.86	50.11
FBD desc	20.66	15.31	25.72	54.91

To examine the effect of h_{rms} and L_c on σ° partial and multiple linear regression analyses were carried out. The partial coefficient R_1^2 reveals the effect of h_{RMS} or L_c on σ° taken independently (Tables 4 and 5). Multiple coefficient of determination R_2^2 shows the percentage of dependence of σ° on h_{rms} and L_c (Table 6). The best relationships between backscattering coefficient and the surface roughness statistical parameters were obtained with logarithmical relations (Figure 4). The maximum values in R_1^2 for both sensors were obtained for h_{rms} which indicate that the influence of σ° on h_{rms} is higher as compared to L_c . For RADARSAT-1, the dependence of σ° on h_{rms} and L_c increased from steeper to shallower incidence (R_1^2 values increased from S2A to S7A). In addition, this dependence did not change with look-azimuth (similar R_1^2 values for S7A and S7D). Under the same polarization, incidence and look-azimuth, the dependence of σ° on h_{rms} and L_c was higher for RADARSAT-1 than for PALSAR. The maximum values of R_1^2 were obtained for PALSAR under HV-pol ($R_1^2 = 0.47$ for h_{rms} , $R_1^2 = 0.42$ for L_c). Finally, it was also detected a slightly improvement of relationship between σ° and both statistical parameters (h_{rms} and L_c) given by highest value for RADARSAT-1 ($R_2^2 = 0.48$) and PALSAR under cross-pol ($R_2^2 = 0.51$).

Table 4. Backscatter coefficients and roughness measurements for surficial geologic units.

Lithologies	hrms (cm)	Lc (cm)	σ° C-HH (F2/Ascend.)	σ° C-HH (S2/Ascend.)	σ° C-HH (S7/Ascend.)	σ° C-HH (S7/Descend.)	σ° L-HH (Descend.)	σ° L-HV (Descend.)
phyllite	0.59	3.69	9.935773	7.534679	10.286707	10.332739	12.7047	21.5151
biotite-hornblende gneiss	2.24	4.85	9.005309	7.610257	9.341192	7.977382	12.431	21.259
quartz-feldspar gneiss	1.75	6.29	7.880478	7.770223	9.534081	9.546896	13.0662	21.3946
biotite-hypersthene gneiss	0.58	5.26	9.49436	8.098635	10.818145	9.341172	13.163	22.1426
biotite-hypersthene gneiss	0.63	3.55	9.428206	5.91677	9.126695	8.276259	12.9038	21.2402
biotite-hypersthene gneiss	0.69	2.66	8.208661	6.996354	8.46861	9.375716	12.3218	21.0487
biotite-hypersthene gneiss	0.43	2.59	9.562754	7.035815	9.10794	7.704614	11.9858	21.3986
migmatite	0.62	3.08	10.56116	6.967604	9.834731	9.624542	12.9974	22.6666
Basic dyke	1.26	6.27	8.750417	8.37749	8.176202	7.438629	12.7075	21.3963
amfibolite	0.58	6.74	10.484297	9.183197	9.426044	9.491995	11.3544	20.3809
pyroxenite	1.46	6.12	12.401352	7.401341	9.249261	9.299668	12.7802	20.5144
biotite-hornblende gneiss	0.26	3.14	10.08094	9.375866	10.304707	10.000401	14.6196	23.0156
pyroxenite	0.99	5.94	8.146413	8.78019	10.196416	9.113845	12.2607	21.7748
Calcic-arenous argillaceous cover	0.30	1.62	14.694201	11.626406	12.456566	10.985933	14.4315	22.8189
Quartz-feldspar gneiss	0.93	3.77	7.499463	7.66731	7.77649	7.862666	11.6265	20.0676
ferruginous quartzite	1.52	5.14	7.613873	7.089703	8.370212	6.672183	12.1267	19.664
Calcic-phyllite	0.30	2.21	12.653997	10.211584	13.262598	11.26725	13.3219	22.5713
phyllite	0.30	1.57	13.689497	11.009534	13.949075	11.432651	14.7121	23.9514

Table 4. Effect of h_{rms} on σ° .

SAR Data		Incidence	$R_1^2 \{ \sigma^\circ = b \cdot \ln(h-rms) + a \}$
RADARSAT-1	C-HH (S2/Ascending)	27.5°	0.32
	C-HH (F2/Ascending)	38.5°	0.38
	C-HH (S7/Ascending)	47°	0.44
	C-HH (S7/Descending)	47°	0.43
PALSAR	L-HH (Descending)	47.5°	0.31
	L-HV (Descending)	47.5°	0.47

Table 5. Effect of L_c on σ° .

SAR Data		Incidence	$R_1^2 \{ \sigma^\circ = b \cdot \ln(Lc) + a \}$
RADARSAT-1	C-HH (S2/Ascending)	27.5°	0.22
	C-HH (F2/Ascending)	38.5°	0.37
	C-HH (S7/Ascending)	47°	0.40
	C-HH (S7/Descending)	47°	0.30
	PALSAR	L-HH (Descending)	47.5°
L-HV (Descending)		47.5°	0.42

Table 6. Effect of both h_{rms} and L_c on σ°

SAR Data		Incidence	$R_2^2 \{ \sigma^\circ = b1 + b2 \cdot \ln(h-rms) + b3 \cdot \ln(Lc) \}$
RADARSAT-1	C-HH (S2/Ascending)	27.5°	0.32
	C-HH (F2/Ascending)	38.5°	0.43
	C-HH (S7/Ascending)	47°	0.48
	C-HH (S7/Descending)	47°	0.44
PALSAR	L-HH (Descending)	47.5°	0.38
	L-HV (Descending)	47.5°	0.51

PALSAR L-HV (Incidence = 47.5°, Look-Azimuth = 282°)

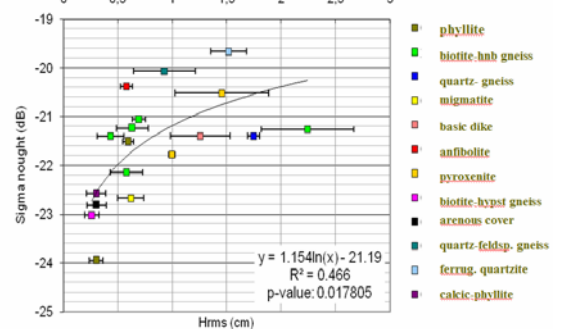


Figure 4 . PALSAR HV σ° (dB) versus h_{rms} with a logarithmic fit ($R_1^2 = 0.466$).

6. Conclusions

Results have shown a weak to moderate linear correlation ($R_2^2 \leq 0.50$) between σ° and micro-topography for RADARSAT-1 and PALSAR. Thus, the use of surface roughness derived from both radar systems is still limited for the characterization of geologic surfaces in the test-site. The best performance of PALSAR with cross-pol (L-HV) was probably due to the influence of the vegetation component with green foliage in the σ° values caused by volume scattering. Further study will be carried out on this subject based on PALSAR and RADARSAT-2 polarimetric data recently acquired in the study area.

Acknowledgments: The authors would like to thank JAXA (ALOS RA 219) and CNPq for a grant received by the first author during this investigation (Process # 300985/90-8).

7. References

- Barbosa, J. S. F.; Sabaté, P. Colagem Paleoproterozóica de Placas Arqueanas do Cráton do São Francisco na Bahia. **Revista Brasileira de Geociências**, v. 33 (1-Suplemento), p. 7-14, 2003.
- Delgado, I. M.; Souza, J. D. **Projeto Cobre-Curaçá: Geologia Econômica do Distrito Cuprífero do Rio Curaçá, Bahia, Brasil**. Salvador: CPRM, 3 vol., 1974.
- Deroin, J.; Company, A.; Simonin, A. An empirical model for interpreting the relationship between backscattering and arid land surface roughness as seen with the SAR. **IEEE Transactions on Geosciences and Remote Sensing**, v. 35, n. 1, p. 86-91, 1997.
- Dierking, W. Quantitative roughness characterization of geological surfaces and implications for radar signatures analysis. **IEEE Transactions on Geosciences and Remote Sensing**, v. 37, n. 5, p. 2397-2412, 1999.
- Kossin, M.; Melo, R.C.; Souza, J.D.; Oliveira, E.P.; Carvalho, M.J.; Leite, C.M.M. Geologia do segmento norte do Orógeno Itabuna-Salvador-Curaçá e Guia de Excursão. **Revista Brasileira de Geociências**, v. 33 (1-Suplemento), p. 15-26, 2003.
- Paradella, W. R. **Discriminação de unidades litológicas no baixo vale do Rio Curaçá (Bahia), através de realces por processamento digital de dados MSS-Landsat 3**. 1983. 250 p. Tese (Doutorado em Geologia) - Instituto de Geociências, Universidade de São Paulo (USP).
- PCI Geomatics 2007. *Geomatica User Guide*. Geomatica Version 10.3, Ontário, Canada: Richmond Hill.
- Rabelo, T. N.; Paradella, W.R.; Santos, A. R.; Rennó, C. D.; Galvão, L.S.; Mura, J.C.; Knust, S. S. A. Evaluating the discrimination of Cu-mineralized rock alteration products from simulated MAPSAR images in the Curaçá Valley, Brazil. **International Journal of Remote Sensing**, v. 28, n. 20, p.4701-4708, 2007.
- Shimada, M.; Isoguchi, O.; Tadono, T.; Higuchi, R.; Isono, K. PALSAR CALVAL Summary (JAXA-PI193). In: First Joint PI Symposium of ALOS Data Nodes for ALOS Science Program, **Proceedings**, Kyoto. Tóquio: Japan Aerospace Exploration Agency (JAXA), 2007. v. CAL-VAL. 4 ps.
- Singh, D.; Singh, P.; Herlin, I.; Sharma, S.K. Ground-based scatterometer measurements of periodic surface roughness and correlation length for remote sensing. **Advanced Space Research**, v. 32, n. 11, p. 2281-2286, 2003.
- Ulaby, F.T.; Bengal, T.H.; Dobson, M.C.; East, J.R.; Garvin, J.B.; Evans, D.L. Microwave dielectric properties of dry rocks. **IEEE Transactions on Geoscience and Remote Sensing**, v. 28, p. 325-336, 1990.
- Ulaby, F.T.; Moore, R.K.; Fung, A.K. **Microwave Remote Sensing: Active and Passive**. Dedham, MA: Artech House, V.II, 1986.
- Verhoest, N. E.C.; Lievens, H.; Wagner, W.; Álvarez-Mozos, J.; Moran, S.; Mattia, F. On the soil roughness parametrization problem in soil moisture retrieval of bare surfaces from Synthetic Aperture Radar. **Sensors**, v. 8, p. 4213-4248, 2008.